Thermal equation of state of tantalum

Ronald E. Cohen [1,2] and O. Gülseren [1,3,4]
[1]*Geophysical Laboratory and Center for High Pressure Research, Carnegie Institution of Washington, 5251 Broad Branch Road, NW, Washington, DC 20015*
[2]*Seismological Laboratory, California Institute of Technology, Pasadena, California 91125*
[3]*NIST Center for Neutron Research, National Institute of Standards and Technology, Gaithersburg, Maryland 20899*
[4]*Department of Materials Science, University of Pennsylvania, Philadelphia, Pennsylvania 19104*
(Received 7 June 2000; revised manuscript received 13 October 2000; published 4 May 2001)

We have investigated the thermal equation of state of bcc tantalum from first principles using the full-potential linearized augmented plane wave (LAPW) and mixed-basis pseudopotential methods for pressures up to 300 GPa and temperatures up to 10 000 K. The equation of state at zero temperature was computed using LAPW. For finite temperatures, mixed basis pseudopotential computations were performed for 54 atom supercells. The vibrational contributions were obtained by computing the partition function using the particle in a cell model, and the finite-temperature electronic-free energy was obtained from the LAPW band structures. We discuss the behavior of thermal equation of state parameters such as the Grüneisen parameter γ, the thermal expansivity α, and the Anderson-Grüneisen parameter δ_T as functions of pressure and temperature. The calculated Hugoniot shows excellent agreement with shock-wave experiments. An electronic topological transition was found at approximately 200 GPa.

DOI: 10.1103/PhysRevB.63.224101 PACS number(s): 64.30.+t, 05.70.Ce, 71.20.Be, 65.20.+w

I. INTRODUCTION

We investigate from first-principles the thermal equation-of-state of body-centered cubic (bcc) tantalum, a group V transition metal, which is a useful high-pressure standard due to its high structural mechanical, thermal, and chemical stability. Ta has a very high melting temperature, 3269 K at ambient pressure, and its bcc structure is stable for a large pressure range. Static diamond anvil cell experiments[1] up to 174 GPa and full-potential linearized muffin-tin orbital (LMTO) calculations[2] up to 1 TPa conclude that the bcc phase of Ta is stable for these pressure ranges. Similarly, shock compression experiments[3] showed melting at around 300 GPa, but no solid-solid phase transition.

II. STATIC EQUATION OF STATE

Firstly, we discuss the static high-pressure properties of Ta, which we obtained from first principles by using the linearized augmented plane-wave (LAPW) method.[4,5] The $5p$, $4f$, $5d$, and $6s$ states were treated as band states, and others are described as core electrons. We used both the local density approximation (LDA)[6] and the generalized gradient approximation (GGA)[7] for the exchange-correlation potential. The Monkhorst-Pack special $\vec{k}$-point scheme[8] with a $16\times16\times16$ k-point mesh (140 k points within the irreducible Brillouin zone of the bcc lattice) was used after convergence tests. The convergence parameter RK_{max} was 9.0, and the muffin-tin radii were 2.0 bohr, giving about 1800 plane waves and 200 basis functions per atom at zero pressure. The total energy was computed for 20 different volumes from 62.5 to 164 bohr^3 (1 bohr$=0.529\,177$ Å), and the energies were fit to the Vinet equation,[9]

$$E(V,T)=E_0(T)+\frac{9K_0(T)V_0(T)}{\xi^2}\{1+\{\xi(1-x)-1\}\times\exp\{\xi(1-x)\}\}, \quad (1)$$

where E_0 and V_0 are the zero pressure equilibrium energy and volume respectively, $x=(V/V_0)^{1/3}$ and $\xi=\frac{3}{2}(K_0'-1)$, $K_0(T)$ is the bulk modulus and $K_0'(T)=[\partial K(T)/\partial P]_0$. The subscript 0 alone throughout represents the standard state $P=0$. All equations of state here are for an isotherm or static ($T=0$) conditions, unless specified otherwise. Pressures were obtained analytically from

$$P(V,T)=\left\{\frac{3K_0(T)(1-x)}{x^2}\right\}\exp\{\xi(1-x)\}. \quad (2)$$

The calculated equation of state is compared with experiments[1,10] in Fig. 1. The LAPW GGA results are found to be more accurate than the LDA. The discrepancies are larger between theory and experiment at high pressures; this may be due to strength effects in the experiments,[11] since we find good agreement with the experimental Hugoniot to 400 GPa (discussed below). For the pseudopotential mixed-basis calculations[12,13] (MBPP, discussed below), we find that the LDA agrees fairly well with the experiments, indicating compensating errors between the pseudopotential and the LDA. Since we are using a first-principles approach, and want to avoid ad hoc variations in procedure to get better agreement with experiments, we use the computational more accurate method with the least approximations, that is LAPW and GGA, rather than the MBPP with LDA, in spite of the fortuitously better agreement of the latter with the room-temperature data.

The residuals between the calculated and fitted energies show large deviations for volumes less than 80 bohr^3 (Fig. 2). Note that the residuals are all small and not evident for

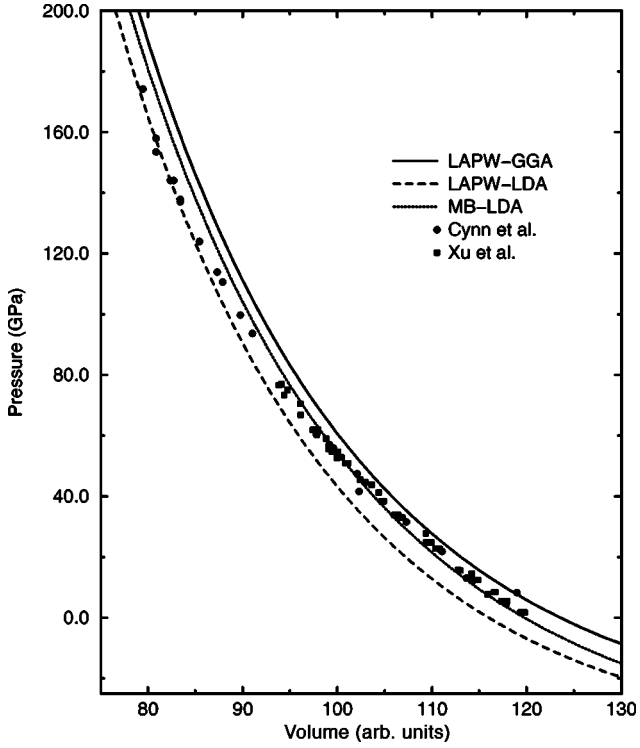

FIG. 1. Static equation of state of Ta. Solid and dashed lines are LAPW, GGA, and LDA calculations, respectively. Pseudopotential mixed-basis results are shown by the dotted line. Circles and squares are two different diamond anvil cell experiments. The discrepancies at high pressures may be due to strength effects in the static equation of state.

the large energy scale shown in Fig. 7(a). Other equation-of-state formulations, such as the extended Birch equation[14] show the same trend.[15] When the fit is restricted to volumes greater than 80 bohr^3, or the Vinet equation is extended by

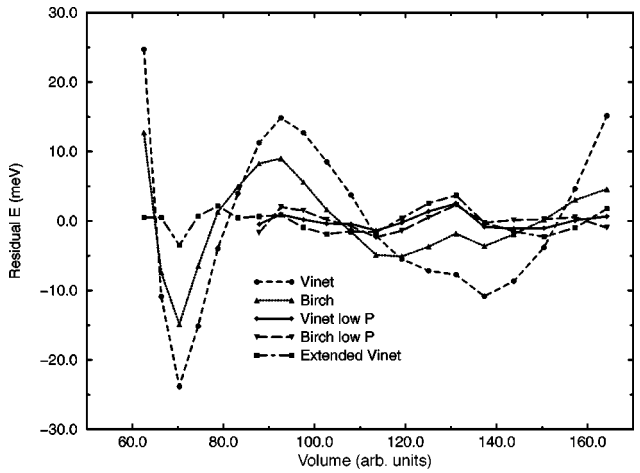

FIG. 2. Energy differences between the calculated and fitted data of the equation-of-state fits. Both Vinet and Birch-Murnaghan equation-of-state fits are shown. In the low-pressure fits only the data with volume greater than 84 bohr^3 were included. The extended Vinet fit included the 2nd and 3rd pressure derivative of $K_0(T)$.

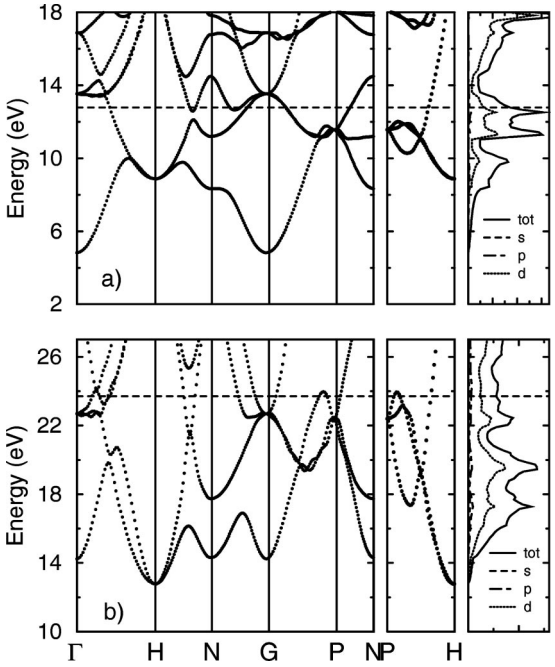

FIG. 3. Band structures and densities of states at two different volumes (pressures): (a) $V=120$ bohr^3 ($P=5$ GPa) and (b) $V=50$ bohr^3 ($P=460$ GPa). Note the significant change in Fermi surface configuration with pressure.

two more parameters related to the next two pressure derivative of bulk modulus, it is improved significantly. Hence, these large residuals are related to different high- and low-pressure behavior of Ta. The band structures and densities of states (Fig. 3) show a major reconfiguration of the Fermi surface. This electronic topological transition is the reason for this change in compression, and the behavior of the residuals for the fitted equations of state. This indicates that systematic deviations from simple equations of state can be used to find subtle phase transitions.[15]

Spin-orbit interactions may be important for Ta. In order to test this, we included spin-orbit coupling by a second variational treatment[16] including 20–80 bands. In contrast to the fully relativistic LMTO results,[2] we found only negligible effect on the equation of state, so our computations were done without spin orbit coupling for the valence states. The core states in CHPW are fully relativistic.

III. CALCULATION OF THERMAL PROPERTIES

In order to compute the high-temperature properties of Ta, we separated the Helmholtz free energy as:[17]

$$F(V,T)=E_{static}(V)+F_{el}(V,T)+F_{vib}(V,T), \qquad (3)$$

where $E_{static}(V)$ is the static zero-temperature energy, $F_{el}(V,T)$ is the thermal free energy from electronic excitations, and $F_{vib}(V,T)$ is the vibrational contribution to the free energy. $E_{static}(V)$ and $F_{el}(V,T)$ were computed using the LAPW method with the GGA. $F_{vib}(V,T)$ was computed using the particle-in-a-cell (PIC) model with a mixed basis pseudopotential method, as described below. The main differences we find between LDA and GGA are in the energy

versus compression, but we find only small differences in energy versus atomic displacements. Since LDA converges much faster than GGA, and is also faster per iteration cycle, we used LDA for the large supercell computations required for the vibrational contributions. Differences from using GGA for this are negligible.

The electronic part $F_{el}(V,T)$ of the free energy is:

$$F_{el}(V,T)=E_{el}(V,T)-TS_{el}(V,T), \tag{4}$$

where $E_{el}(V,T)$ is the internal energy due to thermal electronic excitations,

$$S_{el}(V,T)=-2k_B\sum_i f_i \ln f_i+(1-f_i)\ln(1-f_i) \tag{5}$$

is the electronic entropy, and the Fermi-Dirac occupation f_i is

$$f_i=\frac{1}{1+\exp\left(\frac{[\epsilon_i-\mu(T)]}{k_BT}\right)}, \tag{6}$$

ϵ_i are the eigenvalues, μ is the chemical potential, and k_B is the Boltzmann constant. The vibrational free energy is given in terms of the partition function as

$$F_{vib}(V,T)=-k_BT\ln Z. \tag{7}$$

The particle-in-a-cell model[17,18] was used to calculate the partition function. In this model, the partition function is factored by neglecting atomic correlations. An atom is displaced in its Wigner-Seitz cell in the potential field of all the other atoms fixed at their equilibrium positions, i.e., the ideal, static lattice except for the wanderer atom. The partition function is simply a product of identical functions for all the atoms, involving an integral of Boltzmann factor over the position of a single atom inside the Wigner-Seitz cell,

$$Z_{cell}=\lambda^{-3N}\left\{\int \exp\left[-\frac{[U(\vec{r})-U_0(T_0)]}{k_BT}\right]d\vec{r}\right\}^N, \tag{8}$$

where $\lambda=h/(2\pi mk_BT)^{1/2}$ is the de Broglie wavelengths of atoms and $U(\vec{r})$ is the potential energy of the system with the wanderer atom displaced by radius vector $\vec{r}$ from its equilibrium position. The advantage of the cell model over lattice dynamics based on the quasiharmonic approximation is that anharmonic contributions from the potential energy of the system have been included exactly without a perturbation expansion. On the other hand, since the interatomic correlations between the motions of different atoms is ignored, it is only valid at temperatures above the Debye temperature. Diffusion and vacancy formation are also ignored, so premelting effects are not included. We have used the classical partition function, so quantum phonon effects are not included. Thus the heat capacity and thermal expansivity do not vanish at low temperatures, for example. The present results are appropriate for temperatures above the Debye temperature [245 K in Ta (Ref. 19)] and below premelting effects. Since the Debye temperature is below room temperature in Ta, the classical thermal properties should be reasonable even down to room temperature.

The electronic thermal free energy was obtained using the Mermin theorem[20] [Eq. (5)]. The charge density is temperature dependent through both occupation numbers according to the Fermi-Dirac distribution and self-consistency. The electronic contributions to the thermal-free energy were computed by the LAPW method using the same computational parameters as the $T=0$ K computations described in Sec. II.

For the vibrational contributions, it is necessary to do a large number of large supercell calculations, which is computationally intractable by the LAPW method, but is achievable with the MBPP method.[13] In this mixed-basis approach, pseudoatomic orbitals and a few low-energy plane waves are used as the basis set within a density functional, pseudopotential calculation. It was shown that the method offers a computationally efficient but accurate alternative.

A semirelativistic, nonlocal and norm-conserving Troullier-Martins[21] pseudopotential (with associated pseudoatomic orbitals) was used to describe the Ta atoms. The pseudopotential was generated from a $5d^36s^26p^0$ atomic configuration with cutoff radii 1.46, 2.6, and 3.4 bohr for $5d$, $6s$, and $6p$ potentials, respectively, with nonlinear core corrections. The cutoff radii were optimized by testing the transferability of the pseudopotential by considering the reasonable variations of the reference atomic configuration and by comparing the logarithmic derivative of the pseudowave functions with all-electron values in the valence energy range. The $6s$ potential was chosen as the local component while $5d$ and $6p$ were kept as nonlocal while transforming the potential to the nonlocal separable Kleinman-Bylander form.[22] A full plane-wave representation is used for the charge density and potential, and a smaller cutoff is used for the basis set. The pseudoatomic orbitals are expanded in the large plane wave set for evaluation of the potential and charge density integrals in the Hamiltonian and overlap matrices, and in the total energies. After checking the energy convergence, 550 and 60 eV were used for the large and small energy cutoffs, respectively, in the solid calculations. The exchange-correlation effects of electrons were treated within LDA. The $T=0$ K equation of state of bcc Ta was computed to test the pseudopotential, and is compared with experiment and LAPW results in Fig. 1.

For the PIC computations, a supercell with 54 atoms was used. The MBPP calculations were carried out on this 54 atoms supercell using LDA for exchange-correlations effects and four special $\vec{k}$ points for BZ integrations. The potential energy surface was then calculated as a function of the displacements of the wanderer atom. Symmetry was taken into account in order to reduce the number of computations. The integrand in Eq. (8) has a Gaussian-like shape and decays rapidly, and essentially is zero at half of the interatomic distances even at very high temperatures. Therefore, integration over the Wigner-Seitz cell can be replaced by an integration over the inscribed sphere. Also, the radial part of the integrand is invariant under point group operations of the lattice, hence a numerical quadrature can be used for angular inte-

TABLE I. Vinet parameters for Ta isotherms. The temperatures are odd numbers since computations were done at multiples of $k_BT=0.006$ Ry.

T (K)	$V_0(T)$ (au)	$K_0(T)$ (GPa)	$K_0'(T)$	$E_0(T)$ (Ryd)
0.00	123.63	190.9	3.99	−3 1252.3341
947.32	126.83	163.6	4.31	−3 1252.3665
2052.53	131.38	138.2	4.54	−3 1252.4388
2999.85	135.53	120.5	4.69	−3 1252.5119
3947.17	140.26	103.8	4.83	−3 1252.5925
5052.37	147.30	83.1	5.05	−3 1252.6950
5999.69	155.44	64.5	5.30	−3 1252.7899
6947.01	167.39	45.0	5.64	−3 1252.8917
8052.22	192.24	22.4	6.25	−3 1253.0210
8999.54	230	9.2	6.90	−3 1253.1413
9946.86	289	3.1	7.53	−3 1253.2678

gration based on the method of special directions.[17,23] In this method, the radial integral is expanded in terms of lattice harmonics, cubic harmonics for a cubic lattice, then a quadrature rule is derived for the angular integration in terms of the radial integration by choosing special directions, $\hat{r}_i$, in such a way that the contribution from $l\neq 0$ terms, as many lattice harmonics as possible, is zero. In all of the computations, we used one special direction which integrates exactly up to $l=6$ cubic harmonics.[23] Then, the potential energy was calculated at 4–6 different displacements along this special direction. In order to model the potential, these computed values were fit to an even polynomial up to order 8, which shows the anharmonicity very clearly, since a second-order fit describes the data poorly. Finally, the cell-model partition was calculated from Eq. (8) by carrying out the integration numerically, and the vibrational free energy is simply given in terms of partition function by Eq. (7).

IV. THERMAL EQUATION OF STATE

We treated the resulting free energies[24] three different ways. Firstly, $F-V$ isotherms were fit using the Vinet equation of state, giving $E_0(T)$, $V_0(T)$, $K_0(T)$, and $K_0'(T)$ as the parameters of the fit (Table I, Fig. 4). Because of the thermal expansivity, the minimum energy shifts to higher volumes with increasing temperature, and above $T=6000$ K the $P=0$ volume is not in the range of volumes we studied. The experimental $P=0$ melting temperature is 3270 K, so temperatures above this are nonphysical in any case. The parameters for higher temperatures are fictive parameters that describe the higher pressure equation of state accurately. The Vinet parameters could be fit to polynomials versus temperature to obtain a thermal equation of state, but the following approaches require fewer parameters.

A second thermal equation of state was obtained by analyzing the thermal pressure obtained from the Vinet fits (i.e., the differences in pressures between isotherms). The thermal pressure as a function of volume and temperature is shown in Fig. 5. The volume dependence of the thermal pressure for Ta is very weak up to 80% compression. Deviations at

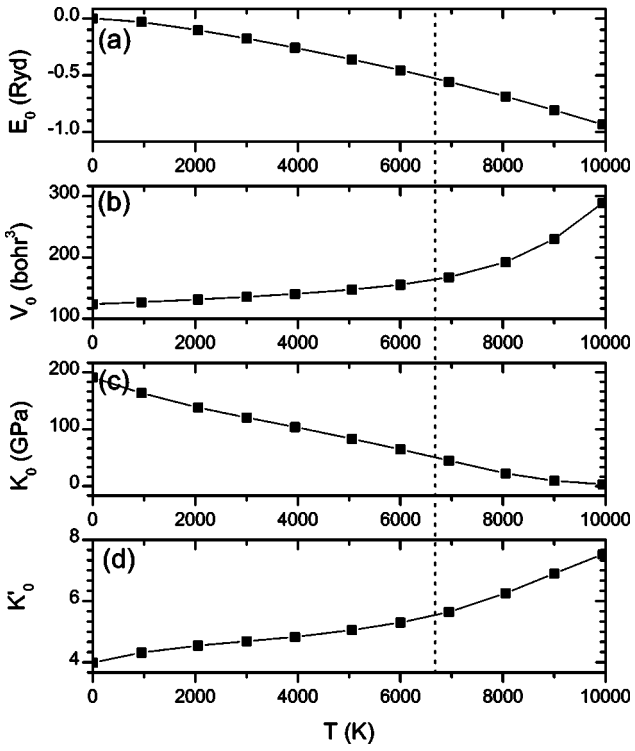

FIG. 4. Vinet equation-of-state parameters as functions of temperature. (a) The minimum energy with respect to the $T=0$ K value $E_0(T=0)=-3$ 1252.33412 Ryd, (b) the equilibrium volume, V_0(T), (c) the bulk modulus K_{T0}(T) at $P=0$, and (d) the pressure derivative of bulk modulus at $P=0$. The vertical line shows the position of the last volume point. At higher temperatures the parameters are fictive, but still govern the high-pressure equation of state.

higher compressions may be due to the fit through the electronic topological transition discussed above, and thus due to inflexibility in the Vinet equation, rather than a real rise in thermal pressure. The thermal pressure is also quite linear in T. The thermal pressure changes are given by

$$P(V,T)-P(V,T_0)=\int_{T_0}^{T}\alpha K_T dT, \tag{9}$$

and αK_T is quite constant for many materials[25] in the classical regime (above the Debye temperature). Hence, a greatly simplified thermal equation of state is to add a thermal pressure

$$P_{th}(T)=aT \tag{10}$$

to the static pressure P_{static}. Since our equation of state is classical, we can use this expression at all temperatures. This simple equation of state gives $q=(\partial \ln\gamma/\partial \ln V)_T=1$ and $(\partial K_T/\partial T)_V=0$, which therefore are good approximations over this pressure and temperature range for Ta.

The thermal pressure was averaged over volumes from 60 to 220 bohr^3, and is shown as a function of temperature in Fig. 6. The solid line has a slope a of 0.00442 GPa/K. This is close to $\alpha K_{0T}(T)$, which is 0.00460 GPa/K at 1000 K and zero pressure. So a simple equation of state for Ta is the static pressure given by V_0 $(T=0)=123.632$ bohr^3, $K_0(T$

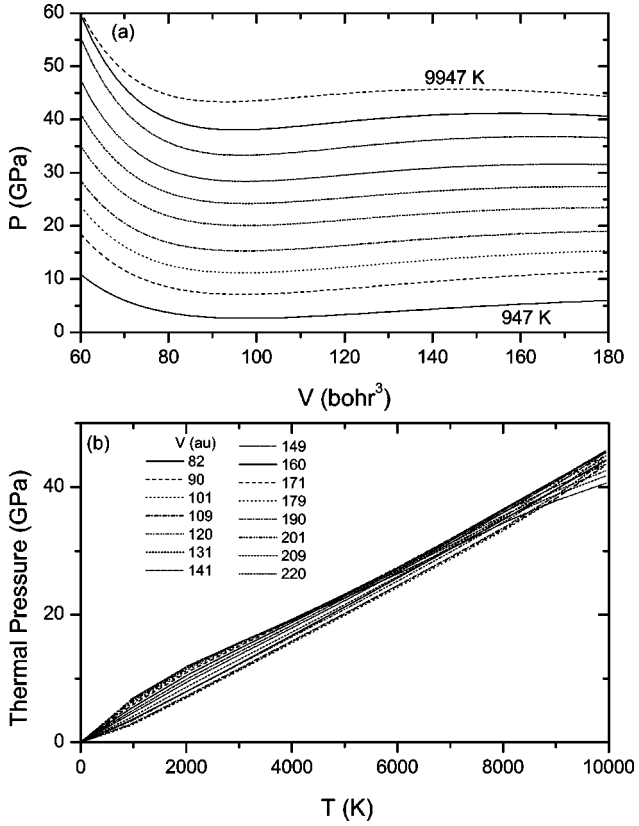

FIG. 5. The thermal pressure as a function of (a) volume at different temperatures (shown in Table I) and (b) temperature from the Vinet fits.

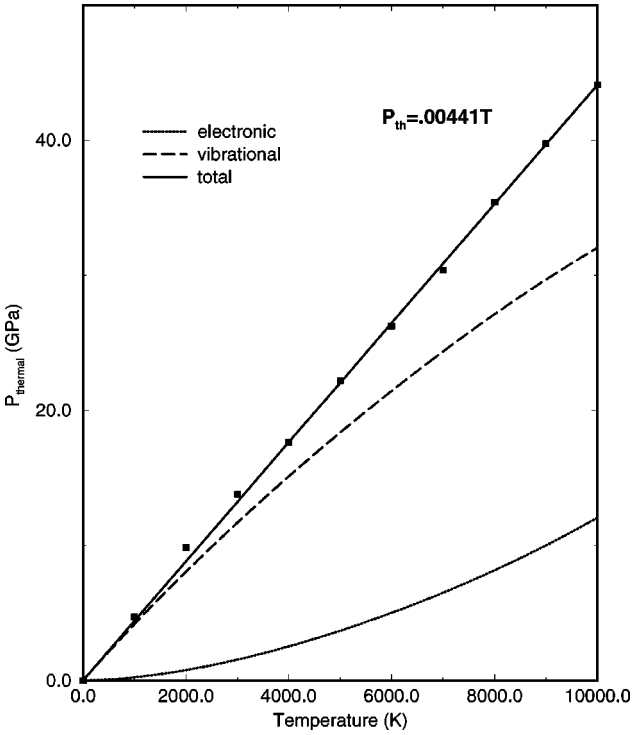

FIG. 6. The thermal pressure averaged over volume as a function of temperature. The solid line is a linear fit with a slope equal to 0.004 42 GPa/K. Also shown are the average vibrational and electronic contributions. The fact that the total is linear, whereas the separate vibrational and electronic contributions are not, must be fortuitous, suggesting that in some systems nonlinear terms in the total thermal pressure may be necessary at very high temperatures.

$=0)=190.95$ GPa, and $K_0'(T=0)=3.98$ in the Vinet equation [Eq. (2)] plus the thermal pressure $P_{th}=0.00442T$.

Thirdly, an accurate high-temperature global equation of state was formed from the $T=0$ K Vinet isotherm and a volume dependent thermal free energy F_{th} as:

$$F_{th}=\sum_{i=1,j=0}^{i=3,j=3} A_{ij}T^iV^j-3k_BT\ln T. \qquad (11)$$

This is the thermal Helmholtz free energy per atom, which must be added to Eq. (1) to obtain the total free energy. The parameters A_{ij} are given in SI units in Table II, which gives the free energy in Joules/atom; T is in Kelvin and V in m^3/atom. The term in $T\ln T$ is necessary to give the proper classical behavior at low temperatures, since we are evaluating the classical partition function, with $C_V=3k_B$ and $S=-\infty$ at $T=0$ K. For the best overall accuracy, the $T=0$ isotherm was also included in the global fit. The global fit is compared with the computed free energies in Fig. 7. The rms deviation of the fit is 0.4 mRy. At low temperatures (0 and 1000 K) the residuals [Fig. 7(b)] are larger due to the elec-

TABLE II. Global fit parameters for Ta in SI units (except where marked). Row is for i and column for j in A_{ij} of Eq. (11). Note that the $T=0$ parameters are not identical to those in Table I, since these were determined from a global fit to all results ($T=0$ and $T\neq 0$) and the Table I values were fit to $T=0$ only. There is no practical difference for applications of these equations of state, within the accuracy of the computations.

	0	1	2	3
1	$2.768\ 10^{-22}$	$-3.295\ 10^{6}$	$6.852\ 10^{33}$	$-1.751\ 10^{63}$
2	$3.734\ 10^{-27}$	-639.6	$2.259\ 10^{31}$	$-4.524\ 10^{58}$
3	$-1.955\ 10^{-31}$	0.0247	$-6.512\ 10^{26}$	$-1.137\ 10^{55}$
V_0	123.52 au	$1.8304\ 10^{-29}$ m^3		
K_0	186.7 GPa	186.7 GPa		
K_0'	4.120	4.120		
E_0	-3 1252.3333 Ryd	$-6.812\,614\,88\ 10^{-14}$ J		

tronic topological transition discussed above (Fig. 2), but at higher temperatures this anomaly is less pronounced due to the thermal smearing, and the equation of state fits well.

Thermal equation of state parameters such as P, α, γ, δ_T, q, and the heat capacity C_V and C_P can be obtained from the global fit by differentiation and algebraic manipulation (see Ref. 25 for a collection of useful formulas.) We now discuss the behavior of these parameters. The thermal expansion coefficient is presented, and compared with zero-pressure experiments[26] in Fig. 8. The deviations at lower temperatures are due to the use of the classical partition function. The thermal expansivity is a quite sensitive parameter, and the errors at moderate temperatures, which are typical in first-principles computations, may come from a number of sources (error in the $P=0$ volume, LDA, the pseudopotential, the PIC model, or convergence in k points or basis set). The divergence in behavior at higher temperatures is not due to vacancy formation, since the vacancy formation in Ta is high (3.2 eV),[27] and the fraction of vacancies at the melting point is less than 10^{-4}. The temperature range over which the anomaly occurs seems too large to be a premelting effect. One possible explanation would be an incipient solid-solid phase transition in Ta, which would not be detected in the PIC method. The upturn in α with increasing temperature is apparently a low-pressure phenomenon. It is possible that it is due to an experimental problem, such as oxidation of the sample.

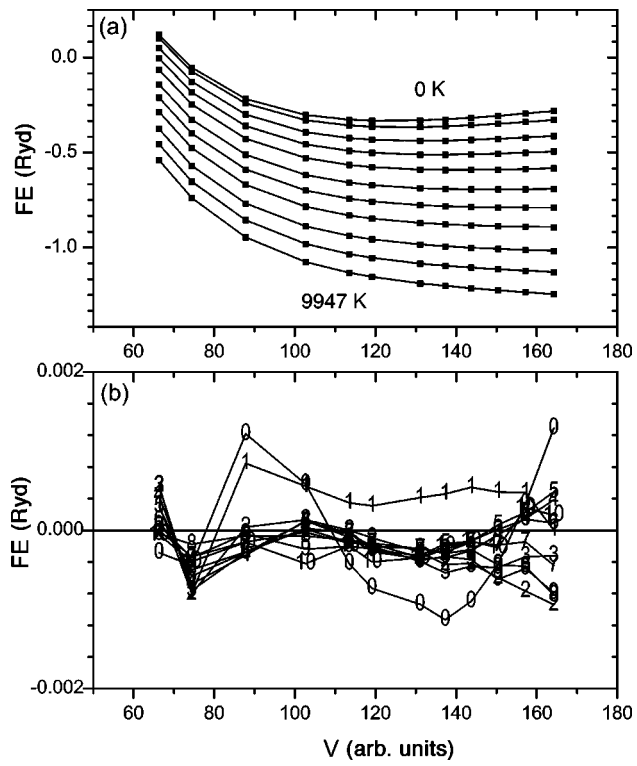

FIG. 7. Global fit to free energies. (a) Computed Helmholtz free energies (symbols) and the result of the global fit (lines) using parameters from Table II. The top curve is for 0 K, and the bottom 9947 K. See Table I for exact temperatures. (b) Residuals of fit. Lines are labeled in order of temperature.

The thermal expansivity drops rapidly with increasing pressure (Fig. 8), and this is parametrized by the Anderson-Grüneisen parameter (Fig. 9)

$$\delta_T = \left(\frac{\partial \ln \alpha}{\partial \ln V} \right)_T . \tag{12}$$

The behavior of δ_T is complex. At low pressures it increases with increasing temperature, but at elevated pressures it decreases with temperature. The parameter δ_T can be fit to a form[28] $\delta_T = \delta_T(\eta=1)\,\eta^{\kappa}$, where $\eta = V/V_0(T_0)$. The average δ_T (averaged from 0–6000 K) decreases with compression, and a power-law fit gives $\delta_T(\eta) = 4.56\,\eta^{1.29}$; at 1000 K $\delta_T = 4.75\,\eta^{1.17}$. Interestingly these values are not that different from MgO (Ref. 28) $[\delta_T(\eta=1,\ 1000\ \mathrm{K})] = 5.00$ and $\kappa = 1.48$. The behavior is much different than for Fe, where δ_T is constant to 150 GPa with values of 5.2 and 5.0 for fcc and hcp, respectively, after which it drops more slowly than a power law.[17] The difference between δ_T and K' is an important anharmonic parameter, and is related to the change in the bulk modulus with temperature at constant volume and the thermal pressure with compression at constant temperature:

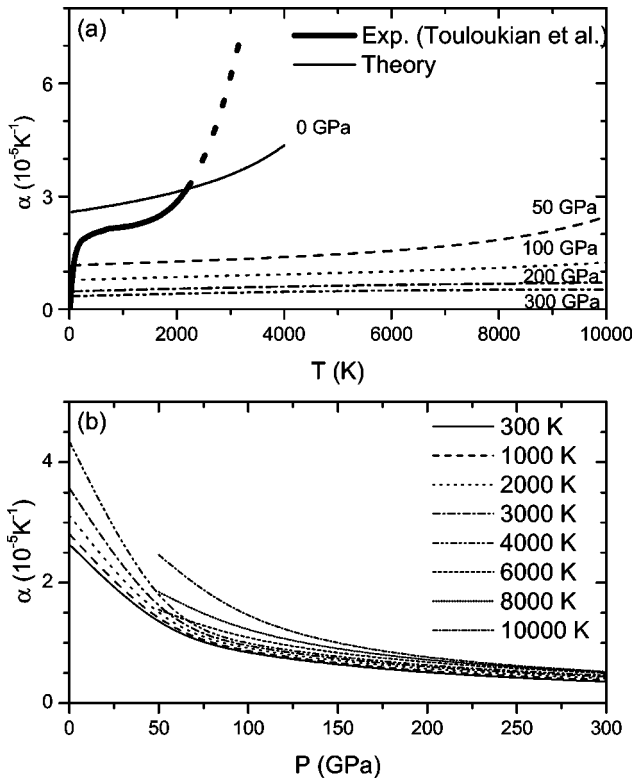

FIG. 8. The thermal expansivity as a function of (a) temperature and (b) pressure. The wide line in (a) shows the experimental zero pressure thermal expansivity (the dashed part is less well constrained). The experimental thermal expansivity shows an anomalous increase at high temperatures. Theory predicts the thermal expansivity to drop rapidly with pressure, and the temperature dependence to decrease.

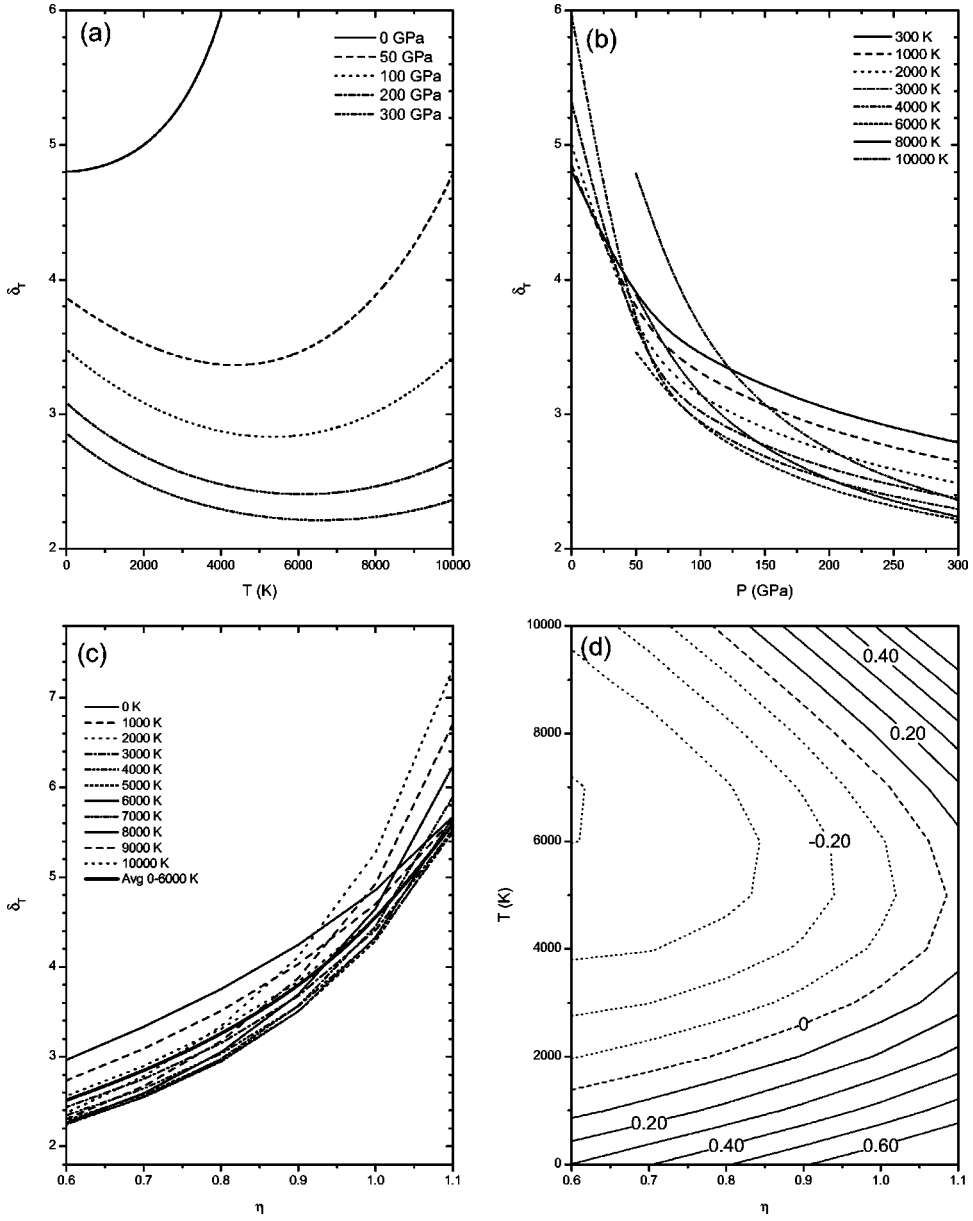

FIG. 9. The Anderson-Grüneisen parameter δ_T as a function of (a) T, (b) P, and (c) $\eta = V/V_0(T=0)$. The average of δ_T from 0–6000 K is also shown as a thick line in (c). (d) Contours of $\delta_T - K'$ show that this quantity is quite small for a large temperature range.

$$\delta_T - K' = \left(\frac{\partial \ln(\alpha K_T)}{\partial \ln V} \right)_T \tag{13}$$

$$= \frac{-1}{\alpha K_T} \left(\frac{\partial K_T}{\partial T} \right)_V . \tag{14}$$

Figure 9(d) shows that $\delta_T - K'$ is quite small over a large temperature and compression range, but increases at high T and P. This is consistent with the accuracy of the simple equation of state [Eq. (10)]. The behavior of $\delta_T - K'$ is also surprisingly similar to the behavior of MgO (see Fig. 3.3 in Ref. 25).

Changes in thermal pressure P_{th} are given by $\alpha K_T = (\partial P/\partial T)_V$ which is shown in Fig. 10. Changes in αK_T are small, but it is interesting that the sign of the change with temperature is strongly dependent on pressure, indicating that experiments to determine $(\partial \alpha K_T/\partial T)$ at low pressures may not be applicable to a very large pressure range.

A most important parameter, particularly for reduction of shock data, is the Grüneisen parameter

$$\gamma = V \left(\frac{\partial P}{\partial E} \right)_V = \frac{\alpha K_T V}{C_V}, \tag{15}$$

where E is the internal energy. The Grüneisen parameter is used in the Mie-Grüneisen equation of state, which assumes γ independent of temperature. Then the thermal pressure on the Hugoniot, for example is given by the change in internal energy by

$$P_{hug} - P_{static} = \frac{\gamma}{V} (E_{hug} - E_{static}). \tag{16}$$

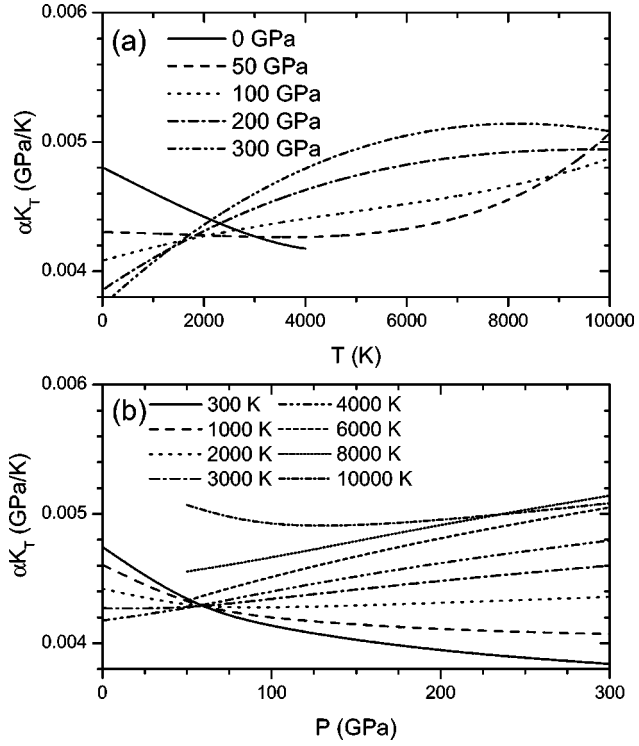

FIG. 10. The dependence of αK_T on (a) temperature and (b) pressure. The temperature dependence of αK_T changes sign with pressure, but the changes are small.

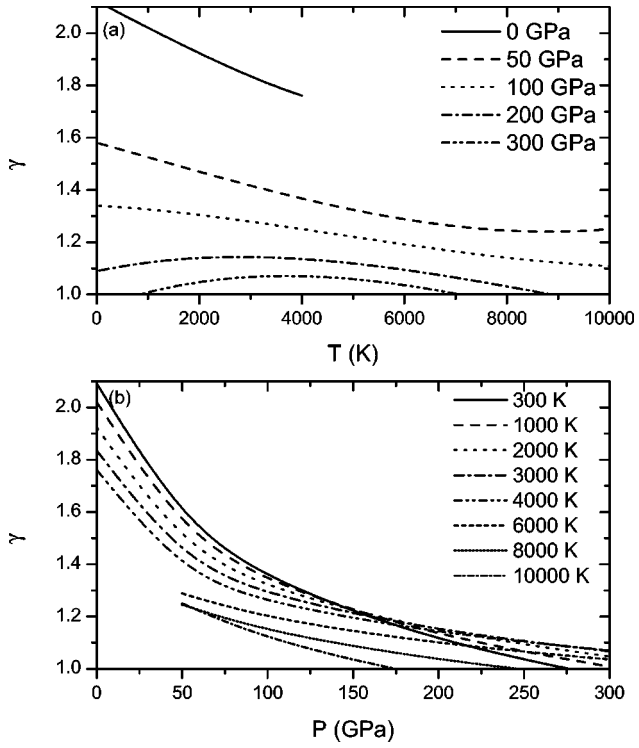

FIG. 11. Variation of the Grüneisen parameter γ with (a) temperature and (b) pressure. The temperature dependence is moderate.

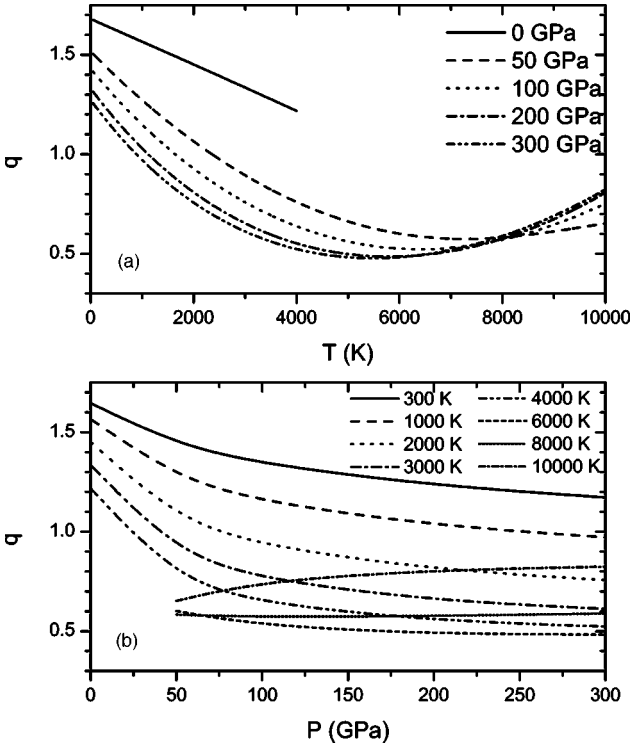

FIG. 12. Variation of q as a function of (a) temperature and (b) pressure. The pressure dependence is small above 50 GPa, but the temperature dependence is significant at all pressures.

Figure 11 shows that at elevated pressures, γ is moderately temperature dependent, and it varies more strongly with temperature below 100 GPa. The variation of γ with pressure is given by

$$q = \frac{\partial \ln \gamma}{\partial \ln V}, \tag{17}$$

which is shown in Fig. 12. The parameter q is not constant, as is often assumed, but decreases significantly with pressure and temperature. If αK_T and C_V were constant, Eq. (15) shows that $q=1$. Figure 10 shows that αK_T is quite constant, so that large changes in q must be due primarily to changes in the heat capacity C_V.

Figure 13 shows indeed that the heat capacity is a strong function of temperature and pressure. This is due mainly to the electronic contributions. The experimental C_P at zero pressure[19] is also shown. Other than the large differences from experiment at very low temperatures, due to neglect of quantum phonon effects in the present model, there is a large increase in the experimental heat capacity with increasing temperature that is not seen in the PIC results. A similar large increase in the experimental thermal expansivity is not predicted by the model (Fig. 8). Vacancy formation (not included in the PIC model) seems an unlikely source for this discrepancy as discussed above. An incipient phase transition or sample oxidation seems the most likely cause of the observed behavior in the thermal expansivity and the heat capacity.

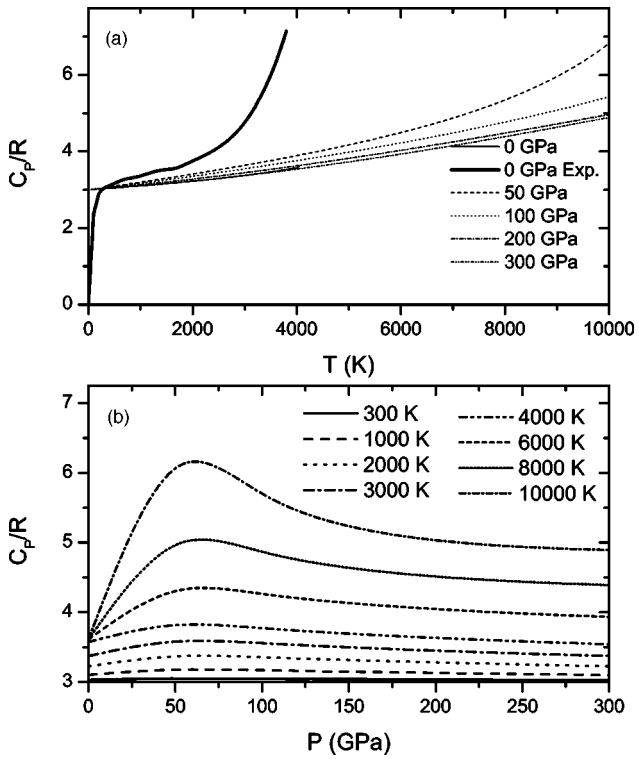

FIG. 13. Variation of the heat capacity with (a) temperature and (b) pressure. The thick curve is the experimental heat capacity (Ref. 19), which shows an anomalous increase at high temperatures, similar to the behavior of the thermal expansivity.

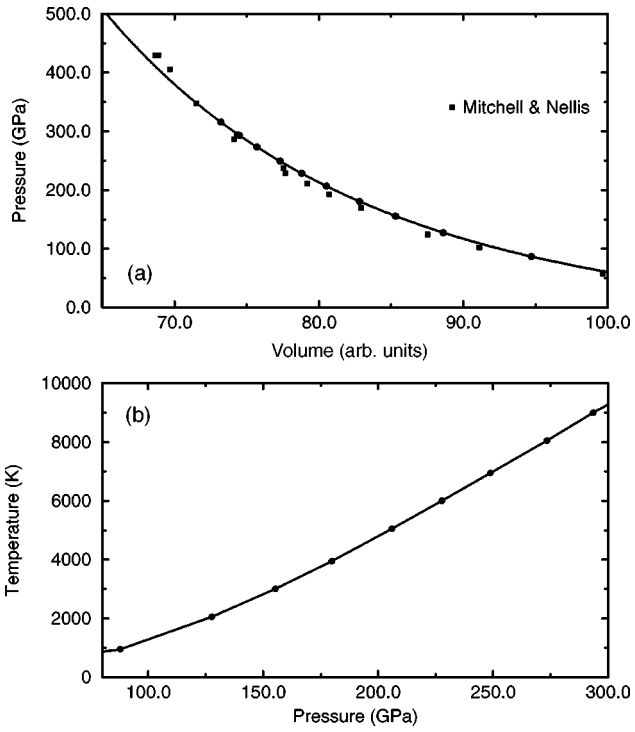

FIG. 14. (a) The line shows the computed Hugoniot for Ta (computed at the points shown as circles). The squares are the shock-wave data (Ref. 3). (b) Theoretical temperatures along the Hugoniot.

To compare with experiment at high pressures and temperatures, we consider the high temperature, high-pressure equation of state obtained by shock compression.[3] The pressures, P_H, and temperatures, T_H, on the Hugoniot of Ta are given by the Rankine-Hugoniot equation:

$$\frac{1}{2}P_H[V_0(T_0)-V]=E_H-E_0(T=0). \tag{18}$$

We solved the Rankine-Hugoniot equation using our equation-of-state results by varying the temperature at a given volume until it was satisfied. The calculated Hugoniot shows very good agreement with experimental data as seen in Fig. 14.

Computations of the Hugoniot using a modified free-volume method were recently presented by Wang *et al.*[29] Though superficially similar to the PIC method, their model is approximate. They included the electronic free energy in the same way that we do, but no supercell is used for the phonon contribution. Instead they find an effective potential from the equation of state of the primitive, one atom unit cell, and integrate the mean-field phonon partition function based on this effective potential. This is a tremendous reduction in effort compared with the use of large supercells and finding the potential for displacing one atom in the supercell. They obtain impressive results for this simple model obtaining excellent agreement with the experimental Hugoniots, not only for Ta, but also Al, Cu, Mo, and W. Nevertheless, it seems unlikely that this simple model will work for lower symmetry systems such as hcp-Fe (Ref. 17) or for elastic constants. For example, the c/a varies with temperature in hcp-Fe, but the Wang *et al.* model would not allow for this.

We summarize the zero pressure 300 K equation-of-state parameters in Table III. The equation of state gives $V(0,T=300\ \mathrm{K})=124.489\ \mathrm{bohr}^3$, 2% higher than the experimental

TABLE III. Thermal equation-of-state parameters at ambient conditions (300 K) (theoretical room-temperature volume and experimental room-temperature volume).

	Theoretical volume	Experimental volume	Experiment
V_0 bohr^3	124.5	(121.8)	121.8 (Ref. 1)
K_{T0} GPa	180	197	194 (Ref. 31)
K'_{T0}	4.2	4.07	3.4 (Ref. 1) and 3.8 (Ref. 31)
α_0 10^{-5} K^{-1}	2.64	2.38	1.95 (Ref. 31)
γ_0	2.09	2.02	1.64 (Ref. 31)
C_P/R	3.03	3.08	3.04 (Ref. 19)

value. Another way of looking at the discrepancy, is that the computed pressure at the room-temperature experimental volume 121.8 bohr^3 is 4.1 GPa rather than 0. Table III also shows the equation-of-state parameters computed at the experimental volume. The main discrepancy is the thermal expansivity which is 35% too high, though this is reduced by comparing at the experimental volume. The Gruneisen parameter is similarly high. The origin of this discrepancy is unknown, as discussed above, although the thermal expansivity (and thus γ) are known to be very sensitive. Apparently this inaccuracy must decrease with increasing pressure, since our Hugoniot agrees well with experiment, up to temperatures of almost 10 000 K. Perhaps our potential surface is not modeled accurately enough at small displacements and low pressures due to the very small energy differences involved in that regime.

V. CONCLUSIONS

We have studied the static and thermal equation of state of Ta from first principles calculations. An electronic topological phase transition is found around 200 GPa. Three different forms of thermal equation of state are provided as: Vinet equation of state with temperature-dependent equilibrium quantities, simple linear temperature-dependent average thermal pressure, and a global fit to the Helmholtz free energy $F(V,T)$. The simple equation-of-state $P_{th}=aT$ works quite well, but more accuracy and insights into higher order thermoelastic parameters were obtained from the global fit in V and T. We find that αK_T is quite constant, as has been seen in experiments for a wide range of materials above the Debye temperatures[25] and has been shown for simple pair potentials.[30] Electronic excitations contribute significantly to the heat capacity temperature dependence of C_V, and thus to variations in the Grüneisen parameter γ. We find good agreement with the experimental Hugoniot and thermal expansivity, though the rapid increase in the thermal expansivity and heat capacity at high temperatures remains unexplained.

ACKNOWLEDGMENTS

This work was supported by DOE ASCI/ASAP subcontract B341492 to Caltech DOE W-7405-ENG-48. Thanks to D. Singh and H. Krakauer for use of their LAPW code. Computations were performed on the Cray SV1 at the Geophysical Laboratory, supported by NSF Grant No. EAR-9975753 and the W. M. Keck Foundation. We thank J.L. Martins, S. Mukherjee, G. Steinle-Neumann, L. Stixrude, and E. Wasserman for helpful discussions.

[1] H. Cynn and C. S. Yoo, Phys. Rev. B **59**, 8526 (1999).
[2] P. Söderlind and J. A. Moriarty, Phys. Rev. B **57**, 10 340 (1998).
[3] A. C. Mitchell and W. J. Nellis, J. Appl. Phys. **52**, 3363 (1981).
[4] S. H. Wei and H. Krakauer, Phys. Rev. Lett. **55**, 1200 (1985).
[5] D. J. Singh, *Planewaves, Pseudopotentials, and the LAPW Method* (Kluwer Academic Publishers, Boston, 1994).
[6] L. Hedin and B. I. Lundqvist, J. Phys. C **4**, 2064 (1971).
[7] J. P. Perdew, K. Burke, and M. Ernzerhof, Phys. Rev. Lett. **77**, 3865 (1996).
[8] H. J. Monkhorst and J. D. Pack, Phys. Rev. B **13**, 5188 (1976).
[9] P. Vinet, J. Ferrante, J. R. Smith, and J. H. Rose, J. Phys. C **19**, L467 (1986); P. Vinet, J. H. Rose, J. Ferrante, and J. R. Smith, J. Phys.: Condens. Matter **1**, 1941 (1987).
[10] J. Xu, H. K. Mao, and P. M. Bell, High Temp.-High Press. **16**, 495 (1984).
[11] T. Duffy *et al.*, Phys. Rev. B **60**, 15 063 (1999).
[12] S. G. Louie, K. M. Ho, and M. L. Cohen, Phys. Rev. B **19**, 1774 (1979).
[13] O. Gülseren, D. M. Bird, and S. E. Humphreys, Surf. Sci. **402**, 827 (1998).
[14] F. Birch, J. Geophys. Res. **57**, 227 (1952).
[15] R. E. Cohen, O. Gülseren, and R. J. Hemley, Am. Mineral. **85**, 338 (2000).
[16] A. H. MacDonald, W. E. Pickett, and D. D. Koelling, J. Phys. C **13**, 2675 (1980).
[17] E. Wasserman, L. Stixrude, and R. E. Cohen, Phys. Rev. B **53**, 8296 (1996).
[18] A. C. Holt, W. G. Hoover, S. G. Gray, and D. R. Shortle, Physica (Amsterdam) **49**, 61 (1970); F. H. Ree and A. C. Holt, Phys. Rev. B **8**, 826 (1973); K. Westera and E. R. Cowley, *ibid.* **11**, 4008 (1975); E. R. Cowley, J. Gross, Z. Gong, and G. K. Horton, Phys. Rev. B **42**, 3135 (1990).
[19] *Handbook of Physical Quantities*, edited by I. S. Grigoriev and E. Z. Meilikhov (CRC Press, New York, 1997).
[20] N. D. Mermin, Phys. Rev. **137**, A1441 (1965).
[21] N. Troullier and J. L. Martins, Phys. Rev. B **43**, 1993 (1991).
[22] L. Kleinman and D. M. Bylander, Phys. Rev. Lett. **48**, 1425 (1982).
[23] A. Bansil, Solid State Commun. **16**, 885 (1975); R. Prasad and A. Bansil, Phys. Rev. B **21**, 496 (1980); W. R. Fehlner, S. B. Nickerson, and S. H. Vosko, Solid State Commun. **19**, 83 (1976).
[24] A table of free energies as functions of T and V is given at http://www.gl.ciw.edu/~cohen/research/taeos.
[25] O. L. Anderson, *Equations of State of Solids for Geophysics and Ceramic Science* (Oxford University Press, New York, 1995).
[26] *Thermophysical Properties of Matter*, edited by Y. S. Touloukian, R. K. Kirby, R. E. Taylor, and T. Y. R. Lee (IFI/Plenum, New York, 1977), Vol. 13.
[27] P. Söderlind, L. H. Yang, J. A. Moriarty, and J. M. Wills, Phys. Rev. B **61**, 2579 (2000).
[28] O. L. Anderson and D. G. Isaak, J. Phys. Chem. Solids **54**, 221 (1993).
[29] Y. Wang, D. Chen, and X. Zhang, Phys. Rev. Lett. **84**, 3220 (2000).
[30] R. J. Hardy, J. Geophys. Res. **85**, 7011 (1980).
[31] K. W. Katahara, M. H. Maghnani, and E. S. Fisher, J. Phys. F: Met. Phys. **9**, 773 (1979).